Laser Beam Welding of Automobile Hinges

A laser welding procedure for joining hinges to the reinforcement structure of car doors is evaluated

BY L. QUINTINO, P. VILAÇA, R. RODRIGUES, AND L. BORDALO

ABSTRACT. Since the establishment of a CO_2 laser beam as a heat source for welding, its application has moved into new areas, replacing existing joining processes. This paper presents an automotive application of laser beam welding for joining hinges to the reinforcement structure of car doors. The objectives of the investigation were to increase productivity, improve repeatability, and maintain overall joint quality, while satisfying the needs for a perfect surface appearance and the structural reliability achieved with the gas metal arc welding (GMAW). Experiments were carried out in two distinct phases. The first dealt with technological feasibility and the second examined the influence of the main laser welding parameters on the quality of the joint. At the end of each phase, nondestructive X-ray and metallographic analyses were applied, allowing the selection of the best overall laser welding conditions. These conditions were then implemented to evaluate the structural integrity of the joints by means of typical automotive industry tests.

Introduction

In a particular automotive plant, hinges were joined to the reinforcement structure of car doors by GMAW. However, the process did not deliver particularly good results. Poor weld appearance was the result of a great amount of spatter. Often the process resulted in nonconformities in quality tests and breaks in production.

In order to increase productivity, repeatability, and overall joint quality, while maintaining the structural reliability, an evaluation of the CO_2 laser beam welding process was initiated. The experimental work was carried out on a lap joint with dissimilar thicknesses and types of parts. The hinge, was made of cast steel, with a thickness increasing linearly from 4.9 to 6.4 mm (0.193 to 0.252 in.). The reinforcement structure was made of rolled steel, 2 mm (0.079 in.) thick, as seen in Fig. 1.

One of the major difficulties in welding these parts was lap joint accessibility. The weld could only be performed from the top surface of the joint on the thicker hinge material. This constraint existed because when the hinge was joined to the reinforcement structure, the door was already assembled, and thus access from the inside was prevented, as seen in Fig. 2.

To obtain adequate penetration and stability of the laser welding keyhole, it is easier to perform the weld from the surface of the thinner part. Normally, where possible, joints are designed that way.

Two other challenges were presented. Lap joint welding was not easy due to the inherent root opening between the parts. Also, the overall thickness from 6.9 to 8.4 mm (0.272 to 0.331 in.) was greater than typical automotive body welding applications.

The first set of experiments was performed on plain steel sheets, while the second set was performed on the actual door reinforcement structure. The results were compiled and analyzed from the selection of the best welded reinforcement structures for structural integrity testing. This testing evaluated not only local joint strength but also overall hinge performance. The tests included shear, peeling, bending, and fatigue tests that simulated normal wear and tear on doors over a long period of service.

KEY WORDS

Laser Beam Welding
Automotive Application
Lap Joint
Dissimilar Materials
Shielding Gases
Porosity

Laser Industrial Applications

Demands for improved production quality, productivity, and flexibility are constantly enlarging the field of laser welding applications (Refs. 1–4). This process is being used for an extensive variety of applications in the automotive, semiconductor, and electronic industries. More recently, it has been used in such diverse fields as medical instruments manufacturing, where heart pacemakers and dental instruments are laser welded, and nuclear and naval equipment, where containers and sheet metal are also laser welded (Ref. 5).

Laser beam welding applications in the automotive industry include welding the roof to the side-panels by a car manufacturer in Ghent, Belgium (Ref. 6). Advantages over spot welding were the formation of a continuous watertight weld, no post treatment required, and less displaced material resulting in better body accuracy. In addition, the problem of welding the zinc-coated material was overcome by carefully selecting weld parameters. Other car manufacturers (Ref. 7) use a laser system to assemble gear transmission shafts, and a particular company (Ref. 8) laser welds automobile roofs using 5-axis CO_2 5-kW laser equipment.

Companies that produce automotive components have also been attracted to laser beam welding for its ability to weld

L. QUINTINO, P. VILAÇA, R. RODRIGUES, and L. BORDALO are with Instituto Superior Técnico (STM), Portugal.

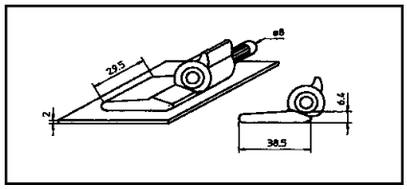

Fig. 1 — Geometry of the lap joint between the hinge (cast steel) and the sheet metal (rolled steel) of the door reinforcement pillar.

Table 1 — Mechanical Characteristics and Norm Specifications of the Parts

Parts	Material	Specification	Yield Strength (N/mm^2)	Tensile Strength (N/mm^2)
Door Reinforcement	Fe P03A	DIN EN 10130:1995	<210	270–350
Hinge	St 52-3	DIN EN 10025:1990	<355	490–630

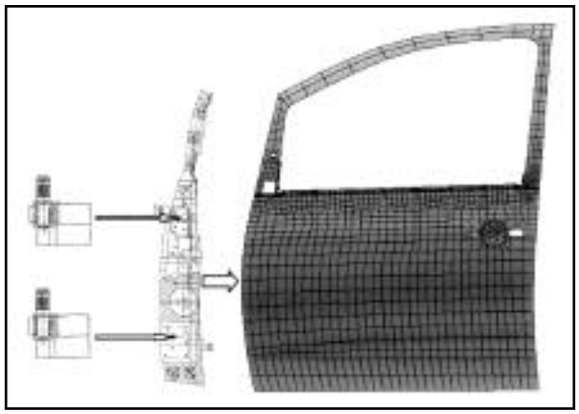

Fig. 2— Schematic of the hinge assembly in the reinforcement pillar of the door structure.

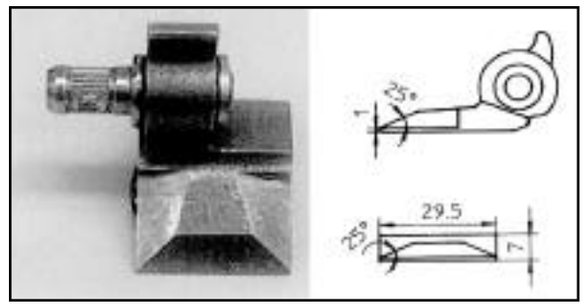

Fig. 3 — The machined hinge geometry intended to overcome the difficulties posed by the original thickness differences of the parts.

premachined precision components with restricted heat input and minimal distortion. The advantages are single-sided access, reduced flange widths and mass, smaller heat-affected zones, less thermal distortion, increased structural strength, high-speed automated processing, and good design flexibility. Generally, a number of CO_2 laser welding applications are now in production for the welding of components such as radiator supports, door window frames, rear shelf panels, and side panels (Ref. 8).

Experimental Procedure

Welding trials were first performed on steel sheets and hinges using original hinge geometry (as distinguished from a machined hinge geometry used later), to investigate different interface preparation conditions. This was followed by trials performed on the actual door reinforcement using the best established interface condition and two different hinge geometries. The selection of the welding parameters was based on visual, nondestructive (radiographic), and metallographic analyses. The most promising conditions were selected for a final test phase aimed at assessing the structural integrity of the assembled joint using typical automotive industry tests.

The method of production of each part influenced the joint fitup. While the hinge was cast, the steel sheet was rolled and then stamped to produce the door reinforcement. The hinge casting produced a rough finish, with a roughness value, R_z (average peak-to-valley height) of about 44 µm, resulting in a gap value between the overlapped parts varying from 0 to about 51 µm. Thus, in order to analyze the gap influence in some hinges, surface preparation was done by grinding it with 1200-grade silicon carbide. The resulting roughness R_z of about 14 µm is equivalent to a fine surface finish of machining processes.

The mechanical characteristics and chemical composition of the materials to be welded are shown in Tables 1 and 2, respectively.

Welds were executed using CO_2 laser equipment capable of generating an output power of 6000 W. In practical terms, this produced a beam net power of approximately 4550 W, with a beam delivery efficiency η = 76%, a focal length of 150 mm (5.905 in.), and a focal diameter of 0.4 mm (0.016 in.). The laser source was operated with continuous wavelength and with multimode TEM, which produced an output that combined several operating modes or profiles. Multimode operation resulted in an increase of output power over that which would be obtained with single-mode operation, but with a partial loss of beam coherence.

The copper nozzle, used for plume suppression conducting the flux of shielding gas, had an outer diameter of 40 mm (1.57 in.), posing a difficult accessibility challenge due to the geometrical configuration of the hinge and reinforcement door structure. As for the handling system, the beam focusing and propagation optics were mounted on a Z-travel axis and the parts to be welded were positioned on an X-Y gantry motion system.

As illustrated in Table 3, the first set of experiments was made, with hinges and plain sheets, using either helium or argon shielding. Using an existing gantry at the work site, a clamping device was adapted to prevent misalignments and to eliminate the gap between the two pieces as much as possible.

The first step was to prove the feasibility of laser beam welding to join the parts present in this specific application. As stated before, one of the main problems was related to the surface finish of the cast hinge, which considerably augmented the joint root opening at the interface. Because of the lap joint configuration, special care had to be taken with maximum

allowable root openings to reduce porosity formation and increase penetration of the keyhole in the sheet. To evaluate the influence of the root opening, a series of hinges were prepared by grinding the surface of the hinge at the interface of the overlapped joint, allowing comparisonof the as-cast and ground surface finishes. To compare these differences, argon was chosen as the shielding gas.

Because a minimized root opening results in deeper penetration and less porosity, ground hinges with original geometry were used to assess the influence of argon and helium as shielding gases on the depth of penetration, without changing the other parameters.

The method for visually selecting the most representative samples was based on a systematic characterization analysis of the following data: laser beam stability (sound and glow from keyhole breakdowns and/or plasma formation), width of the weld bead at the top surface (measured value), penetration (total/partial), clear burned-edges (yes/no), general shape of the bead at the top surface (convex/plan/concave), and spatter (many/few/none). After selecting the most representative samples, X-radiography tests were made to reveal possible porosity, cavities, or cracks in the weld metal, as well as to determine which hinges were to be metallographically examined, and, within these, which were the most critical cross sections. Consequently, the most representative and important samples were cut, mounted, polished, and etched for subsequent microscopic analysis.

As a result of the first set of experiments, a combination of helium gas and ground hinges was selected for the trials undertaken in the second set of experiments on the reinforcement structure. The number of welded hinges is described in Table 3.

At this point, different hinge geometry was introduced to reduce the thickness of the weld bead, as seen in Fig. 3.

Both hinge geometries were welded on the original door reinforcement, which demanded the use of a new fixture. The best welding parameters achieved during the first set of experiments on sheet steel were used as a starting condition for the second set. Moreover, the group of parameters resulting from the second set of experiments, during which the hinges were welded to the original door reinforcement structure suffer only minor variations in comparison to the final ones from the first set.

Weld beads were also made starting and finishing inside the hinge, as seen in Fig. 4. When starting welding inside the hinge, special care was taken with delay times. The time had to be long enough to develop a keyhole, but it could not be too long since this would excessively melt the parts and produce a melt-through. A delay interval ranging from 0.5 to 1 s was used.

The second fixture was designed and built to firmly hold the door reinforcement. The aspects of repeatability and positioning accuracy were taken into account when designing this device, as well as the possibility of welding both geometrical conditions of the hinge. The machined hinge was rotated 25 deg from the horizontal working plan to maintain the perpendicular position between the laser beam and the surface of the hinge. The geometry and clamping characteristics of the fixture are illustrated in Fig. 5.

To guarantee correct placement of each pair of hinges on their respective door reinforcement, the hinges had to be aligned on the same axis to allow proper door rotation. The holding device between the parts is represented in Fig. 6.

As in the case of the first set of experiments, radiographs were made on visually representative samples to reveal possible defects in the weld. Once more, representative samples were prepared for metallographic analysis.

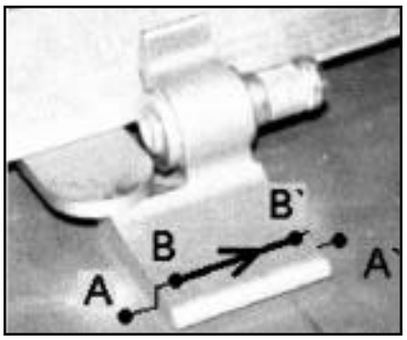

Fig. 4 — Schematic of the two different paths for the welds. AA — Across the hinge, starting and finishing inside the plain sheet; BB — starting and finishing inside the hinge.

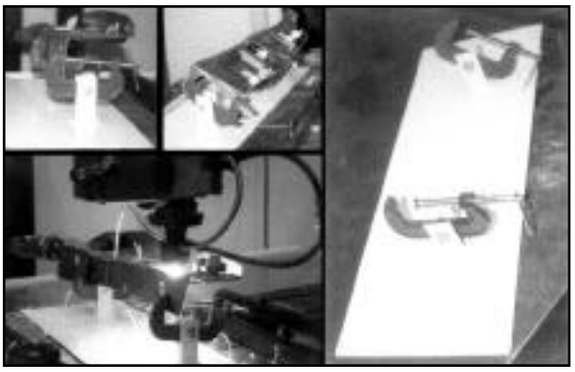

Fig. 5 — The gantry geometry used during the second set of experiments allows different angular positions for the clamping device of the door reinforcement pillar.

Table 2 — Chemical Composition of the Hinge and Door Reinforcement Materials

	Chemical Composition (%)					
Material	C	Si	Mn	P	S	Al
FeP03A (door reinforcement)	0.1	—	0.45	0.035	0.035	0.2
St 52-3 (hinge)	0.2	0.55	1.6	0.035	0.035	—

Note: FeP03A — rolled steel; St52-3 — cast steel.

Table 3 — Overall Experiment Conditions for All Welding Trials Performed

		1st Set of Experiments (hinge joined to plain sheet)		2nd Set of Experiments (hinge joined to reinforcement structure)	
Hinge geometry		Original		Original	Machined
Surface finishing		As cast	Ground	Ground	
Shielding gases	Argon	20	34	—	—
	Helium	—	10	14	6
		Number of welded Hinges			

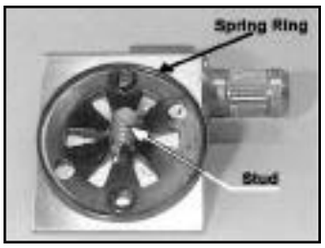

Fig. 6 — To firmly hold the hinges to the door reinforcement and to ensure the smallest gap between them, a stud was welded to the base of the hinge and a spring ring was used to fasten it.

Analysis of Results

Visual inspection of both sets of experiments revealed a satisfactory appearance of all weld joints where argon was used as a shielding gas. There was even better superficial finishing with helium shielding, which produced more stable and narrower welds with a convex upper bead.

Seven samples, representative of the different conditions (Table 3), were selected for detailed analysis from the welds made in both sets of experiments. These were the welds on which the best visual appearance, penetration level and stability were achieved. The corresponding weld parameters and overall conditions of these samples are described in Table 4. The only samples that had spatter were those with the largest weld bead widths, as seen in Table 5.

In fact, the only samples selected that exhibited spatter, Ar2 and He2, were those with higher heat input and lower velocity values, as confirmed in Fig. 7.

It is well known (Ref. 8–12) that obtaining weld beads with less width, higher velocity values should be used. This increases keyhole stability and also results in less porosity formation.

In examining the radiographic results (Table 6), a difference was found between ground and nonground hinge surface finishing. The amount and size of porosity was very significant for the nonground or as originally cast hinge surface finish. This behavior was the trend obtained for all 20 trials performed. The ground surface not only produced a better fit and less energy loss by reflection/refraction of the beam at the gap on the interface of the overlapped parts but also hydrogen sources like the hydroxide layer present at the surfaces, were greatly reduced by careful surface preparation procedures. The final grinding grade and respective cleaning, for example, were applied immediately before welding executions.

The sample Ar2, welded under exactly the same conditions as Ar1 but with a ground surface, was intended to emphasize this phenomenon, as seen in Fig. 8.

In order to complete the analysis of the porosity formation and other important characteristics, such as the penetration obtained in all the experiments, it is necessary to introduce the metallographic analysis results — Table 7, Fig. 9.

Concerning porosity formation when using argon shielding and lower welding speeds, two types of porosity were encountered. First, some very large bubbles

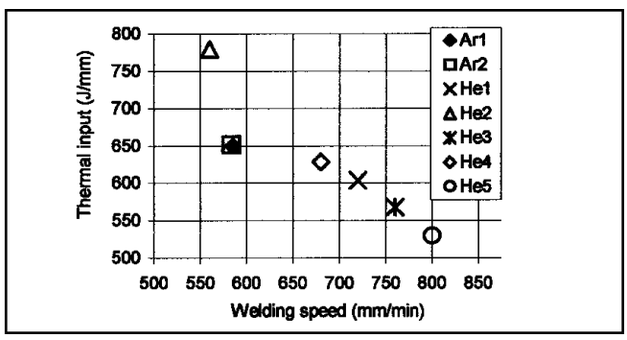

Fig. 7 — Nominal heat input vs. welding speed for all selected samples. The best results were achieved for higher welding velocities.

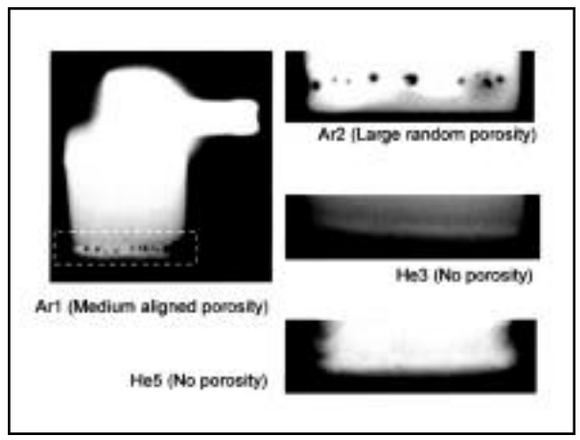

Fig. 8 — Some representative X-ray results of the selected samples. Porosity and lack of total penetration were investigated.

Table 4 — Weld Parameters and Overall Conditions of the Most Representative Samples of Both Sets of Experiments

Sample	Hinge Geometry	Hinge Surface Finishing	Hinge Joined To:	Power (W)	Weld Speed (mm/min)	Shielding Gas	Flow Rate (l/min)	Total Thickness (mm)	Heat Input (J/mm)
Ar1	original	nonground	plain sheet	5000	585	Ar	15	7	390
Ar2	original	ground	plain sheet	5000	585	Ar	15	7	390
He1	original	ground	plain sheet	5720	720	He	20	7	362
He2	original	ground	plain sheet	5740	560	He	20	8.4	467
He3	original	ground	reinforcement	5680	760	He	20	7	341
He4	machined	ground	reinforcement	5620	680	He	20	6.6	377
He5	machined	ground	reinforcement	5570	800	He	20	6.6	317

Observation: All welds were performed usingTEM multimode; stand-off = 6 mm; focal position = 0 mm.

Table 5 — Results of the Visual Aspect Analysis of the Selected Samples

Sample	Spatter	Bead Width at Top Surface (mm)
Ar1	None	5.0
Ar2	Few	5.4
He1	None	4.5
He2	Few	5.3
He3	None	4.4
He4	None	3.3
He5	None	3.1

Table 6 — Results of the Nondestructive X-Ray Tests of Selected Samples

Sample	Porosity Quantification	Dimension	Pattern
Ar1	Many	Medium	Center aligned
Ar2	Some	Large	Random
He1	Many	Small	Center aligned
He2	Some	Little	Random
He3	No porosity	—	—
He4	Few	Little	Random
He5	No porosity	—	—

were located randomly along the thickness direction of the weld. Second, smaller centerline porosity occurred in cases where full penetration was not accomplished.

The authors believe that in the first case, it was mostly hydrogen-induced porosity and porosity formed by the unstable evaporation of the metal over the front wall of the keyhole (Refs. 8, 13, 14). In the second case, it was also present under the protection of a helium environment (as can be seen in the He1 photomacrograph), possibly due to keyhole instability caused by the fact that full weld penetration was not achieved (Refs. 13, 14). More generally, it is possible to conclude that in all the experiments performed, small centerline porosity located near the toe of the weld bead corresponded to cases of incomplete penetration.

With helium shielding and slightly higher welding speeds, macro- and aligned porosity were almost eliminated, but smaller pores could be detected by microscopic examination, both on the weld center and near the weld interface. This reduction in porosity formation and size was due to the stabilizing effect on the keyhole caused by increased welding speeds. The higher the welding speed, the more stable the weld pool; therefore, less gas (air, shielding gases, and plasma) was introduced and the trapped gas, including metal vapor, could escape more easily.

Porosity was located either at the centerline or randomly distributed through the fusion zone, with a tendency for concentration near the weld interface. Centerline porosity was caused by the entrapment of gas bubbles during solidification and pushed by advancing dendrites. The porosity located near the weld interface consisted of bubbles trapped at the beginning stage of solidification (due to the high cooling rate). This occurs in the most stable location where a gas can exist inside of a liquid phase, at the solid/liquid interface, where the surface tension of the pore surface was at a minimum.

Concerning distribution of porosity through the thickness, porosity was located from the bottom to the top zone, depending on the location of precipitation and on the width-to-penetration ratio of the weld bead. This can be observed in Fig. 9, where sample Ar2 and He2 have a width-to-penetration ratio, respectively, high and low, resulting in a different porosity location. Thus, the main controlling parameter was weld velocity, because under low values of this parameter, the weld pool was significantly wide, indicating a conduction mode as opposed to a narrow one resulting from a stable keyhole mode.

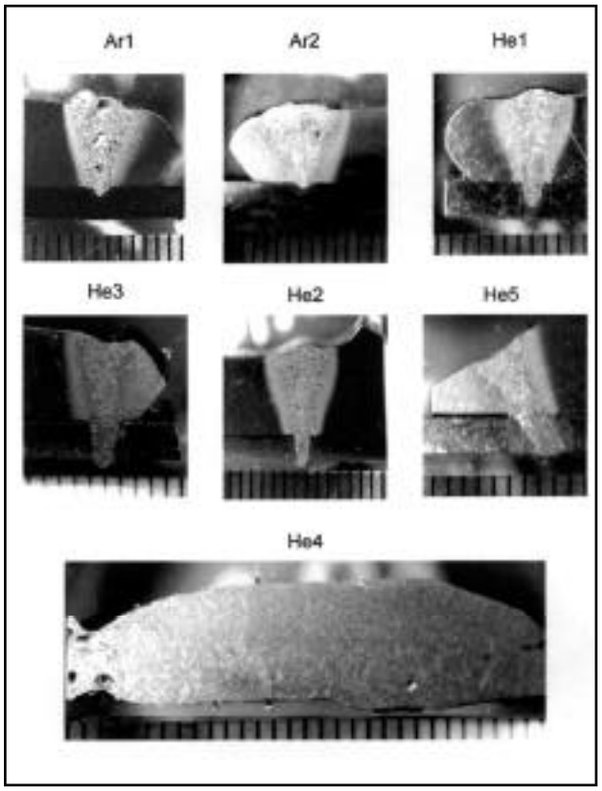

Fig. 9 — Macrographs of cross sections of selected samples. Penetration level, porosity location along the thickness, and HAZ extension are characterized.

Full penetration levels were accomplished only with helium. With argon, incomplete penetration was encountered, despite the use of lower welding speeds. This was confirmed by the macrographs shown in Fig. 9. The explanation for this phenomenon is the previously mentioned plasma plume formation with argon shielding that resulted in significant energy absorption. As helium is less likely to form this plasma, the energy absorbed by the parts is higher, resulting in greater penetration.

One of the main characteristics of overall weld quality is the width and nature of the crystalline structure formed in the heat-affected zone (HAZ). The measurement of the HAZ width comes as a result of the metallographic analysis, present in Table 7. Since determining the nature of the HAZ is not included in the scope of this work, only the width values will be discussed.

Comparing samples Ar1 and Ar2, which were welded with the same heat input, the following conclusions about the influence of two different interface conditions in the overall characteristics of the welds, *e.g.*, porosity formation, penetration level, and HAZ width can be made.

The most significant differences between these two samples were porosity formation, which for Ar2 was less than for Ar1, and penetration level which was greater for Ar2 than for Ar1. These results were probably due first to the surface cleaning effect of the grinding process and the consequent removal of hydroxides frequently responsible for porosity formation in laser welding. Secondly, the most efficient contact between the overlap parts resulted in lower thermal resistance and inferior losses in the power of the beam when it reached the root opening.

The HAZ obtained for Ar2 shows a width with 0.2 mm (0.008 in.) more than the HAZ width for Ar1, which should not be relevant in terms of metallurgical characteristics and resulting residual stress field.

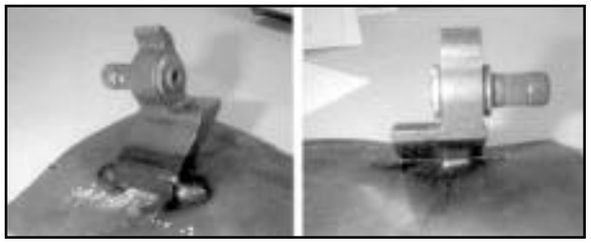

Fig. 10 — Front and back view of the joint after tear-down test.

Fig. 12 — Outside view shows the pneumatic cylinder that activates the handle, opening the door latch for the crazy chicken fatigue test. The system of door push and pull is located inside, closing with a 25 g acceleration force. The complete cycle takes about eight seconds to accomplish.

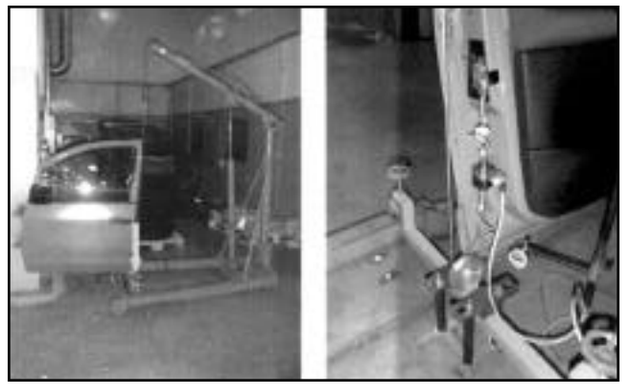

Fig. 11 — General and detailed view of the sagging test apparatus with force sensor and digital caliper to measure flexion.

Fig. 13 — Upper hinge deformation, top left door deformation, and top right door deformation, respectively.

The comparison between HAZ widths applies only to samples welded under the same conditions of hinge geometry, surface finishing, shielding gas, and flow rate. In addition to the previous example, it is possible to directly compare only the samples He1 and He3, which have been welded under heat inputs of 362 and 341 J/mm (9194.8 and 8661.4 J/in.) respectively. According to expected behavior, the higher heat input value corresponded to the greater width HAZ, as observed in Table 7.

Maximum penetration occurred when the beam was focused slightly below the top surface of the lap joint. To find the limit interval, the authors tried to lower the point as much as possible to compensate for the power deficit in order to achieve a full penetration weld. The limit was found when the focal point was so deep into the part that no keyhole mode was formed and a transition to conduction mode welding occurred. Results showed that when the focal point position was higher than 0.5 mm below the hinge surface, not only did the keyhole become unstable, but also its start up was more difficult. This behavior may be due to the degradation of the power density at the top surface of the parts to be welded.

For the focal point positioned above the top surface of the hinge, no stable keyhole mode was achieved, probably due to the decreasing power density of the beam when it reached the surface. Thus, reliable and repeatable results were obtained for a focal point location with a depth up to 0.5 mm (0.0197 in.) below the surface.

It is relevant at this stage to summarize the best overall conditions achieved at the end of all the trials performed. Samples chosen were the He3 and He5, as seen in Fig. 7. These samples had higher welding velocity and lowest heat input for the original and machined hinge geometry. These characteristics corresponded to total penetration, no porosity formation, and more stable and narrower welds with a convex upper bead.

Mechanical Tests

After the welding trials established the optimum welding conditions, mechanical tests were carried out to assess the structural integrity of the joint. First, a tear-down test, was done to evaluate the shear strength of the joint. Next, the flexion test ("sagging") was done to assess the flexibility resistance. Finally, the fatigue test ("crazy chicken") was done to simulate the intensive use of a normal production car door.

The crazy chicken and sagging tests required complete doors. Two laser-welded hinges (He3) were chosen to perform these mechanical tests.

From the two samples selected in the previous section, He3 and He5, a decision was made to test only original hinges. This explains why samples with the same characteristics as He5 were not tested.

After the hinges were welded to the door reinforcement pillar, the two selected doors were completely assembled. Because it is the most used of a car's four doors, the driver's door was chosen for testing.

Tear-Down Test

This test is usually done to validate spot and GMA welds. It consists of introducing a pneumatically activated chisel into the lap joint to tear the parts apart. The test is designed to evaluate if the assembly will fail at some constant applied force rather than to find the force at which the assembly fails. The magnitude of this constant force is based on experience.

The pneumatic chisel, with a 7.5 bar (0.75 MPa) pressure, was then inserted on the backside of a single-weld hinge to sever the laser welded joint, disconnecting the parts.

If inserting the chisel on the backside of the hinge did not break the parts, just deformed the steel sheet, the chisel was then introduced on the frontside of the

hinge, acting directly on the weld. The final result was the steel sheet tore completely while leaving the weld intact, as seen in Fig. 10. In this case, the backside of the hinge was completely raised due to the plastic deformation of the less resistant steel sheet.

Flexion Test

This test assesses the door flexion resistance by the application of a series of vertical loads to the lock end of the door, measuring the elastic and plastic deformation at the hinges. The test specification requires a maximum plastic deformation of 1.5 mm (0.059 in.) for a 1000 N (224.8 lbf) load.

According to test requirements, the door has to be opened 5 deg and suspended by the two hinges when applying the load. Then, load is applied to the lock, pulling the door vertically down, as represented in Fig. 11.

Due to the existence of just one weld, a stress concentration, was created around the weld when it was loaded, which caused bending of the steel sheet (structurally weaker than the hinge) and consequently augmented the total deformation. If this had been a normal production door test, the door would have failed, as the maximum plastic deformation of 1.5 mm was achieved for a load of about 700 N, *i.e.*, inferior to the 1000 N, for which the total plastic deformation was about 18 mm. The hinge deformation occurred only at the upper hinge, since this was the one subjected to tension loading, while the lower one is in compression.

The results show that the ultimate strength was not attained till 1700 N (382.2 lbf). Since this behavior occurred with just one weld, it may be expected that if two parallel welds were used on the hinge, the static strength and deformation would not be a problem.

Fatigue Test

The fatigue test involved opening and closing a car door up to 100,000 cycles. The test is controlled by pneumatic cylinders, which opens the door from the outside and pushes from the inside, opening it completely — Fig. 12. Then the latter, using a cable, pulls the door and closes it.

After working for approximately 20 h, the test stopped after 8,666 cycles due to the deformation of the steel sheet. The door warped, which interfered with its closing, as seen in Fig. 13. The sensor then actuated and cut the power to the PLC controlling hardware.

It is emphasized that joint did not break in the welded zone, either by overload or fatigue. The test stopped at such an early stage strictly because of the door steel sheet deformation. It is expected if the hinges had been welded with two parallel welds, the test results would have been totally positive. As previously explained, this was not possible due to spatial-related constraints.

Conclusions

The results allow the following conclusions:

Surface finish of the parts makes a great difference in the amount of porosity formation with laser beam welding. With improved surface preparation, this phenomenon can be significantly reduced.

Helium was found to be the most suitable gas for this application since it increased overall heat efficiency.

The machined weld preparation delivered a distinct improvement, allowing a weld procedure with higher velocities and lower heat input while maintaining total penetration of both hinge and door reinforcement structure.

As expected, higher welding speeds contributed to keyhole stabilization and, consequently, less porosity and a thinner weld bead.

Typical hydrogen-induced porosity was reduced through careful grinding of the surface with reduced the hydroxide layer, a hydrogen source.

As for focal point location, a depth up to 0.5 mm (0.0197 in.) below the surface provided reliable and repeatable results.

Although only a single laser beam weld was made on the hinges mechanically tested, the weld bead did not fail, nor was there any sign of weakness.

The performance of the doors mechanically tested was limited by plastic deformation in the welded parts and was not limited by the mechanical strength of the joint. Failure occurred by deformation of the base metal due to an uneven stress distribution in the hinge assembly, resulting from the fact that one of the hinges edge was welded, while the other remained free to move.

The procedure developed accommodated all the fabrication needs, *e.g.* surface finishing, access restrictions and duration of the operation, using a commercially available 6-kW CO_2 laser system.

Acknowledgments

This work was supported by AutoEuropa-Automóveis, Lda., the Volkswagen car plant in Palmela-Portugal.

The authors would like to thank Instituto de Desenvolvimento e Inovação Tecnológica (IDIT) Feira-Portugal, the technology institute where all the laser welds were performed, and the Portuguese Welding Institute ISQ for their support.

References

1. Lancaster, J. F. 1986. *The Physics of Welding.* pp. 185–191, The International Institute of Welding.

2. Norrish, J. 1992. *Advanced Welding Processes.* Institute of Physics Publishing Ltd., pp. 185–199.

3. Nippes, E. F. 1983. Welding, brazing and soldering. *Metals Handbook*, 9th edition, Vol. 6, ASM Handbook Committee, pp. 647–671.

4. Welding processes 1991. *Welding Handbook*. Vol. 2, 8th edition, American Welding Society, Miami, Fla., pp. 713–738.

5. Santos, J. O., Quintino, L. 1998. *Processos de Soldadura* (Welding Processes), Portuguese Welding Institute (ISQ), pp. 579–632.

6. Holt, T. 1995. New applications in high power laser welding. *Welding & Metal Fabrication*, 63(6): 230–234. Fuel & Metallurgical Journals Ltd.

7. Kunzig, L. 1994. Laser welding of automotive and aero components. *Welding & Metal Fabrication*, 62(1): 14–16, Fuel & Metallurgical Journals Ltd.

8. Gonçalves, V. 1997. Soldadura laser de ligações dissimilares (laser welding of dissimilar joints). Ph. D dissertation, Technical University of Lisbon, pp. 47–78.

9. Metzbower, E. 1993. Keyhole formation. *Metall. Transactions* B, 24: 875–880.

10. Arata, Y. 1986. *Plasma, Electron and Beam Technology — Development and Use in Material Processing*. pp. 378-396. ASM International, Materials Park, Ohio.

11. Dowden, J., Kapadia, P., Postacioglu, N. 1989. An analysis of the laser-plasma interaction in laser keyhole welding. *Journal of Physics D.*, 22(6): 741–749, Applied Physics.

12. AGA AB. 1997. *Facts about Laser Welding Gases*, ed. Beskriv Tecknik AB, Lidingo.

13. Matsunawa, A., Kim, J., Seto, N., Mizutani, M., Katayama, S., 1998. Dynamics of keyhole and molten pool in laser welding. *Journal of Laser Application*, 10(6): 247–254, Laser Institute of America.

14. Matsumoto, T., Fukuda, N., Kondo, Y., Ohmoni., A., Inoue, K., Arata, Y. 1999. Study on prevention of welding defects in high power CO_2 laser materials processing. *Journal of Laser Application*, 11(6): 258-262, Laser Institute of America.